Inelastic neutron scattering study of anharmonic interactions in orthorhombic $KNbO_3$

R. Currat
Institut Laue-Langevin, 38042 Grenoble, France

H. Buhay* and C. H. Perry
Physics Department, Northeastern University, Boston, Massachusetts 02115

A. M. Quittet†
Laboratoire de Physique des Solides, Universite Paris–Sud, 91405 Orsay, France
(Received 16 June 1989)

Inelastic neutron scattering studies have been performed on ferroelectric $KNbO_3$ in its orthorhombic phase at room temperature. Dispersion curves up to 10 THz have been determined for phonons propagating along the [101], [010], and [111] pseudocubic directions. A detailed intensity map of the inelastic response from the B_2-symmetry TA, TO1 (soft), and TO2 phonon branches has been constructed. The scattering profiles collected at $(1+\zeta,3,1+\zeta)$, with $0.02<\zeta<0.25$, are analyzed using a phenomenological mode-coupling model. The uncoupled mode frequencies, linewidths, structure factors, and coupling parameters are determined. Good internal consistency is achieved assuming a mode-coupling mechanism of the interaction-damping type. The present analysis resolves existing discrepancies between neutron and Raman scattering results on the zone-center frequency of the TO1 (ferroelectric) mode.

INTRODUCTION

The dynamical properties of the orthorhombic phase of ferroelectric $KNbO_3$ have been studied extensively by diffuse x-ray,[1] inelastic neutron scattering,[2] Raman scattering,[3–8] and infrared[5,9] spectroscopy. Currat *et al.* using neutron scattering investigated the acoustic and low-frequency optical-phonon branches.

Their observations provided the basis for much of the work that followed.[10] In particular, they reported a steeply rising transverse-optical (TO1) phonon branch and a transverse-acoustic (TA) branch propagating along the ferroelectric axis ([101] direction in pseudocubic notations), and polarized along [010]. They associated the zone-center frequency of the TO1 branch with the "ferroelectric" B_2 mode, i.e., the uncondensed component of the high-temperature cubic F_{1u} soft mode.

In constant-energy scans at $\mathbf{Q}=(1-\zeta,3,1-\zeta)$, the TO1 branch was observed as a sharp intensity ridge for $\zeta>0,1$, merging into the wing of the intense TA branch for $\zeta<0.1$. The authors concluded that the TO1 mode was overdamped at low q's, and by extrapolation of the high-q spectra, they estimated the zone-center TO1 frequency to be 0.7 ± 0.1 THz (23 ± 3 cm^{-1}).

Room-temperature Raman scattering studies by several groups indicated that, in the region below 250 cm^{-1} (7.5 THz), the spectrum of B_2 symmetry was dominated by a broad intensity peak (TO1) around 37 cm^{-1} (1.1 THz). A sharp feature with an antiresonance line shape (TO2) was observed at 200 cm^{-1} (6.0 THz). A coupled-mode line-shape analysis produced quasiharmonic frequencies of 57 cm^{-1} (1.7 THz) and 195 cm^{-1} (5.8 THz), with corresponding linewidths of 85 cm^{-1} (2.6 THz) and <5 cm^{-1} (0.15 THz).

The discrepancy between Raman and neutron scattering results for the lower mode frequency (TO1), had led to some controversy concerning the interpretation of the Raman scattering spectra. In particular, Scott[11] has proposed to interpret the 57-cm^{-1} Raman scattering peak as a disorder-induced one-phonon density of states peak. On the other hand, the correctness of the Raman scattering analysis was subsequently confirmed by infrared reflectivity measurements,[9] which yielded quasiharmonic frequencies and linewidths for the TO1 and TO2 modes in good agreement with the Raman scattering results.

In this work we present a room-temperature inelastic neutron scattering study of various low-frequency (0.5–10 THz) phonon branches, propagating along the [101], [010], and [111] directions (standard pseudocubic notations are used throughout; see, Ref. 2). Particular attention is given to the line-shape analysis of the transverse-acoustic (TA) and two transverse-optical modes (TO1 and TO2) of B_2 symmetry, propagating along the [101] ferroelectric axis and polarized along [010]. A phenomenological mode-coupling model is used to reproduce the observed neutron intensity profiles for selected wave vectors $\mathbf{q}=(\zeta,0,\zeta)$. The dispersion of the decoupled mode frequencies and linewidths are extracted from the fits, together with the wave-vector variation of the coupling parameters.

Specifically, we find that the dispersion of the TO1 branch is significantly shifted from the position of the intensity maxima in the measured spectra. This is due to the large intrinsic linewidth of the T01 mode at small q and to the strong anharmonic interaction between this mode and the TA branch of the same symmetry. The

decoupled quasiharmonic frequency of the TO1 branch, when extrapolated to $q \rightarrow 0$, agrees well with a similar analysis of the Raman scattering spectrum.

EXPERIMENTS

A 1.5-cm^3 single crystal of $KNbO_3$, grown by the top-seeded flux technique, was provided by E. Wiesendanger, ETH, Zurich, Switzerland. Electrical poling of the crystal at a temperature just below the tetragonal-orthorhombic phase transition (488 K), resulted in an essentially monodomain orthorhombic structure.

All neutron scattering measurements were performed at room temperature using the IN8 three-axis spectrometer at the Institute Laue-Langevin, Grenoble, France. The spectrometer was operated in the down-scattering mode with a fixed outgoing neutron wave vector of $k_F = 3.3$ Å^{-1} ($E_f = 5.0$ THz). Cu(111) and Cu(220) crystals were used at a monochromator and pyrolytic graphite (002), as analyzer . With the collimations used, the resulting instrumental linewidth was in the range 0.3–0.5 THz FWHM.

Potassium niobate at room temperature is orthorhombic with space group $Bmm2$ (C_{2v}^{14}). Because the orthorhombic distortion is weak, it is convenient to refer the structure to the principal axes of the parent cubic phase. With such (pseudocubic) notations, the spontaneous electrical polarization lies along [101] and the ferroelectric soft mode is polarized along [010] (B_2 symmetry). Zone-center modes polarized along [101] and [10$\bar{1}$] are labeled A_1 and B_1, respectively. In the present experiment the crystal was mounted with a (hkh) horizontal scattering zone.

DISPERSION CURVES

The measured phonon dispersion curves are summarized in Fig. 1. The different symbols in the figure refer to the various Brillouin zones in which the data were collected. For the phonon branches propagating along [101] and polarized along [010] [(TA, TO1, and TO2 branches in Fig. 1(b)], the frequencies shown in the figure have been obtained via a mode-coupling analysis described in the following sections. In the other cases, the mode frequencies were obtained directly from the observed peak positions.

The TO1 mode is strongly polar and exhibits a large angular dispersion in the limit $q \rightarrow 0$: for q along [101] the extrapolated zone-center frequency corresponds to the B_2 mode at ~ 1.8 THz, whereas for q along [010] the TO1 branch extrapolates to a zone-center mode of A_1 symmetry at 290 cm^{-1} [$=8.7$ THz; not shown in Fig. 1(a)]. As the propagation vector is rotated from [101] towards [010], the extrapolated zone-center frequency varies continuously between the above two limits (see Fig. 2 in Ref. 12). This is illustrated in Fig. 1(c) for the case of the [111] direction.

In contrast, the ionic displacement involved in the TO2 mode are only weakly polar and the polarization direction remains parallel to [010] for all propagation directions. Hence, as q rotates from [101] to [010], the character of the mode changes from B_2-TO to B_2-LO. The LO frequency is slightly lower than the TO one, due to the negative sign of the dielectric constant $\epsilon_2'(\omega)$ in the TO2–LO2 frequency range.[13] The dielectric constant is dominated by the contribution of the ferroelectric mode whose LO component lies at ~ 420 cm^{-1} (12.7 THz), i.e., well above the LO2–TO2 frequency range.

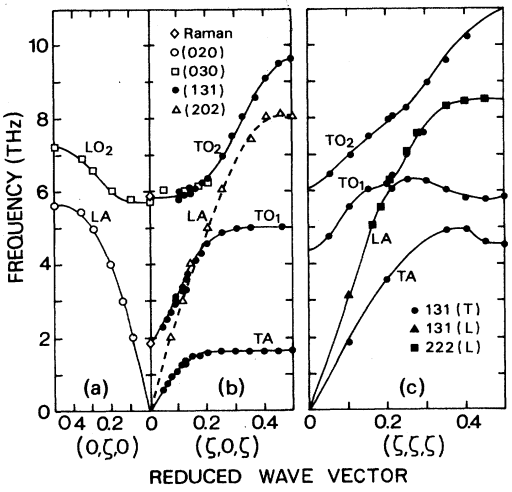

FIG. 1. Phonon dispersion curves in orthorhombic $KNbO_3$ at room temperature. The symbols refer to the Brillouin zones used in the measurements. Raman scattering data are shown as open diamonds.

The anisotropy of the TA branch has been discussed previously.[2] In particular, it has been shown that the plateau frequency at 1.6–1.7 THz in Fig. 1(b) corresponds to the vibration along [010] of the Nb ions alone. A similar plateau at the same frequency is observed for all propagation directions in a reciprocal plane normal to [010]. When q is rotated away from this "soft" plane the TA frequency rises sharply, a behavior which leads to the appearance of diffuse streaks on x-ray photographs.[1]

The microscopic mechanism which gives rise to the TA anisotropy is the same as that which leads to ferroelectric soft modes and ferroelectric instabilities. This is expected from the close connection between the eigenvectors of the B_2-TO1 soft mode and that of the TA branch in the plateau region. Also, the temperature behavior of the two branches is similar: At the orthorhombic-to-rhombohedral phase transition (~ 210 K), both anomalous features disappear simultaneously, i.e., the B_2-TO1 frequency increases abruptly and the x-ray streaks disappear.

In the high-temperature cubic phase three sets of diffuse x-ray streaks are observed, corresponding to propagation directions normal to the three degenerate ⟨100⟩ polarization directions. This feature is common to many oxydic perovskites, whether they undergo ferroelectric instabilities as $KNbO_3$ and $BaTiO_3$, or only exhibit a ferroelectric soft mode and a large dielectric susceptibility as $KTaO_3$. The anisotropic and nonlinear electronic polarizability of the O^{2-} ions provides a common microscopic mechanism behind the above experimental observations.[14–16]

ANHARMONIC EFFECTS

The perovskite compounds which undergo ferroelectric transitions have highly overdamped soft modes in the high-temperature cubic phase.[17–20] As a consequence, the ferroelectric transition (cubic-to-tetragonal) is generally discussed in terms of order-disorder models with relaxational-type dynamics.[1,8,21]

In $KNbO_3$ at room temperature and below, anharmonic damping effects are less severe and a simple soft-mode description appears to be adequate. Nevertheless, some care must be exercised in extracting quasiharmonic frequencies from experimental neutron spectra. This point is well illustrated in Fig. 2 which shows a raw intensity contour map taken in the (131) Brillouin zone. The upper and lower intensity ridges are associated with the TO1 and TA branches of Fig. 1(b). However, due to damping and mode-coupling effects, the quasiharmonic mode frequencies do not coincide with the position of the intensity ridge in the raw data. Failure to appreciate this point has led the authors in Ref. 2 to seriously underestimate the value of the zone-center TO1 frequency (0.7 THz).

The first step in analyzing the data shown in Fig. 2 consists in reducing them to a set of constant-Q spectra. This is shown in Fig. 3 where the same data are replotted together with data not included in Fig. 2 and covering the TO2 frequency range ($\omega > 5$ THz).

The data in Fig. 3 show the broad TO1 response with wings overlapping the sharp TA and TO2 modes. Since all three branches are of the same symmetry, we have a situation where anharmonic interference effects are potentially significant and should be accounted for in the data analysis.[22]

Several authors have derived expressions for the spectral response function from coupled harmonic oscillators, in the context of lattice dynamics. Barker and Hopfield[23] have used a coupled-mode analysis in discussing the infrared reflectivity spectrum of several cubic perovskites. Asymmetrical Raman scattering line shapes due to anharmonic interference effects have been reported in orthorhombic $KNbO_3$ by several groups.[3,5,6] Harada *et al.*[17] have observed TA-TO1 interference effects in cubic $BaTiO_3$, using inelastic neutron scattering.

The line-shape distortions which are observed here are not as severe as in the case of cubic $BaTiO_3$, in view of the lower degree of damping of the TO1 branch present here. In fact, an approximate fit of the spectra in Fig. 3 can be achieved using independent damped harmonic oscillators [see Fig. 4(a)]. However, a definite improvement is obtained in the overlap regions by introducing coupling

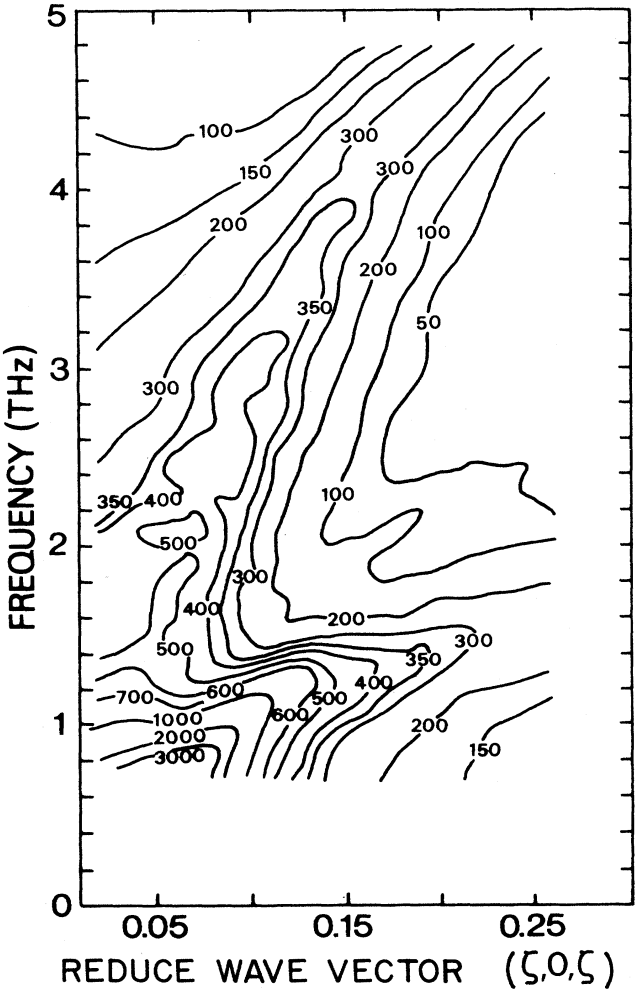

FIG. 2. Neutron intensity map derived from constant-energy scans in steps of 0.1 to 0.2 THz between 0.7 and 5 THz. The data were taken in the (131) Brillouin zone along the [101] direction: $Q=(1-\zeta,3,1-\zeta)$.

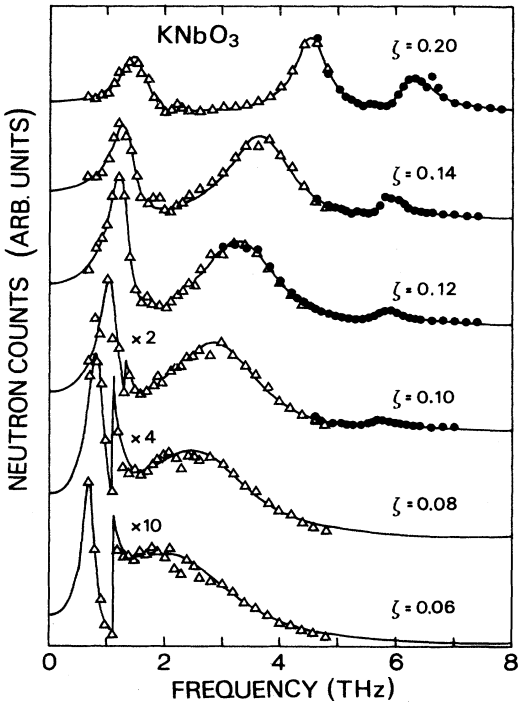

FIG. 3. Constant-Q scans at $Q=(1-\zeta,3,1-\zeta)$. The triangles refer to data points replotted from Fig. 2, and the circles to additional constant-Q measurement. Lines are guide to the eye.

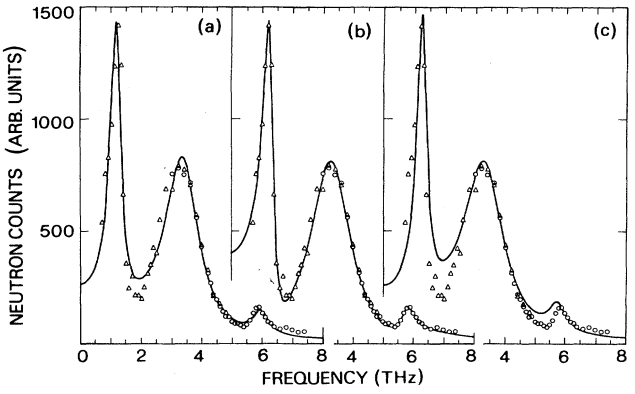

FIG. 4. Damped harmonic oscillator analysis of constant-Q data ($\zeta=0.12$): (a) independent oscillator fit; (b) coupled oscillator fit with imaginary coupling; and (c) effect of mode interactions: The solid line is calculated with the same values as in (b) for the free-mode parameters and with coupling parameters set to zero.

parameters between TO1 and TA, and between TO1 and TO2 [see Fig. 4(b)].

MODE-COUPLING ANALYSIS

Following Wehner and Steigmeier[24] the spectral intensity $I(\omega)$ for the case of two modes in terms of the retarded phonon Green's function g_{ik} and the inelastic structure factors S_i is given by

$$I(\omega)=[n(\omega)+1]\sum_{ik}(2\omega_i)^{1/2}S_i(2\omega_k)^{1/2}S_k\,\mathrm{Im}g_{ij}(\omega)\ , \tag{1}$$

where $n(\omega)=[\exp(h\omega/kT)-1]^{-1}$ denotes the Bose-Einstein function.

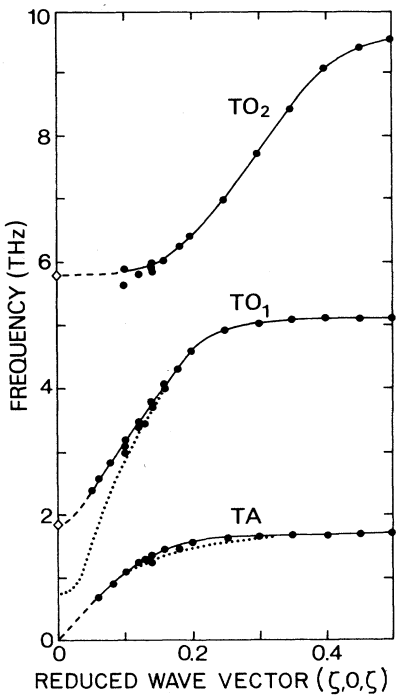

FIG. 5. Decoupled quasiharmonic frequencies derived from the coupled oscillator analysis. Raman scattering results at $\zeta=0$ are shown as open diamonds. The dotted lines refer to the position of the intensity maxima in Fig. 2.

The explicit form obtained for Eq. (1) for a single pair of interacting modes is

$$I(\omega)=[n(\omega)+1]\left[\frac{CY-BZ}{B^2+C^2}\right]\ , \tag{2}$$

where

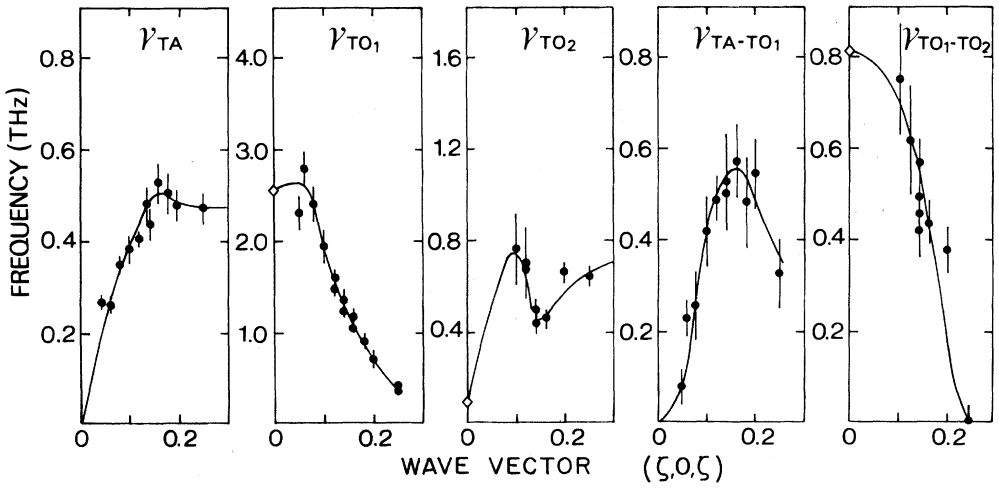

FIG. 6. Best-fit damping and coupling parameters derived from the coupled oscillator analysis (imaginary coupling). Raman scattering results at $\zeta=0$ are shown as open diamonds.

TABLE I. TO1 free-mode parameters as deduced from the analysis of the TO1-TA (a) and TO1-TO2 (b) coupled-mode response, assuming dissipative coupling in both cases [S: inelastic structure factor in arbitrary units; ω: quasiharmonic mode-frequency (THz); γ: damping coefficient (THz)].

	S_{TO1} (a.u.)		ω_{TO1} (THz)		γ_{TO1} (THz)	
ζ	(a)	(b)	(a)	(b)	(a)	(b)
0.10	42.7±1.0	43.3±0.5	3.08±0.05	3.17±0.05	1.95±0.15	1.95±0.10
0.12	42.2±1.0	42.5±0.5	3.41±0.03	3.44±0.03	1.60±0.10	1.64±0.05
0.14	41.4±1.0	41.7±0.5	3.71±0.03	3.77±0.02	1.38±0.10	1.36±0.05
0.16	37.6±1.0	38.7±0.5	4.04±0.03	4.03±0.02	1.17±0.10	1.08±0.05
0.20	33.8±1.0	33.5±0.5	4.51±0.03	4.56±0.02	0.73±0.05	0.68±0.05
0.25	26.1±1.0	24.7±0.5	4.91±0.03	4.91±0.02	0.41±0.05	0.36±0.03

$$B=(\omega_1^2-\omega^2)(\omega_2^2-\omega^2)+\omega^2(\gamma_{12}^2-\gamma_1\gamma_2)-\omega_1\omega_2\Delta_{12}^2 ,$$

$$C=\omega[\gamma_1(\omega_2^2-\omega^2)+\gamma_2(\omega_1^2-\omega^2)-2(\omega_1\omega_2)^{1/2}\Delta_{12}\gamma_{12}] ,$$

$$Y=S_1^2(\omega_2^2-\omega^2)+S_2^2(\omega_1^2-\omega^2)-2S_1S_2(\omega_1\omega_2)^{1/2}\Delta_{12} ,$$

$$Z=\omega(S_1^2\gamma_2+S_2^2\gamma_1-2S_1S_2\gamma_{12}) .$$

The four parameters ω_1, ω_2, S_1, and S_2 (the frequencies and structure factors) and the four parameters γ_1, γ_2, Δ_{12}, and γ_{12} (free-mode damping constants and coupling coefficients between the modes) in Eq. (2) define an eight-parameter model for the spectral intensity for two coupled oscillators.

Equation (2) contains one parameter more than can be determined uniquely from the spectrum $I(\omega)$. This indeterminacy is due to the arbitrariness in subdividing the total energy of the system into a free-mode energy and an interaction energy. For each spectrum an infinity of eight-parameter sets exist and transformations can always be found such that either Δ_{12} or γ_{12} is transformed to zero.[23] The justification for using either real (Δ_{12}) or (γ_{12}) imaginary coupling in the analysis of a given spectrum must be based on additional physical arguments.

In the present case, the choice concerning the type of coupling to be used is *a priori* open. Although most authors have found it convenient to use imaginary coupling in analyzing optical spectra from perovskite compounds, one may expect real coupling to dominate in the low-frequency limit.[17] The unique aspect of the data in Fig. 3 lies in the fact that they show *one* mode (TO1) which interferes separately with *two* others (TA and TO2). It is readily seen that in such a case the arbitrariness in using Eq. (2) is removed and the nature of the coupling mechanisms can be identified.

Practically, the analysis was performed as follows: The scans corresponding to $\zeta=0.10$, 0.12, 0.14, 0.16, 0.20, and 0.25 were fitted twice using Eq. (2). In each case the frequency range was selected in such a way as to cover only one of the two overlap regions. Satisfactory fits could be obtained with either real (springlike) or imaginary (dashpotlike) couplings. However, only in the latter case did the two sets of best-fit TO1 free-mode parameters come out of to be mutually consistent. The results for S_{TO1}, ω_{TO1}, γ_{TO1} are shown in Table I. The composite result of the calculation (using average values for the TO1 parameters) is shown as full lines in Fig. 4.

At low-q values, the structure factor of the TO2 mode vanishes and its interference with the TO1 mode cannot be analyzed. The scans corresponding to $\zeta=0.05$, 0.06, and 0.08 were fitted under the assumption of imaginary TO1-TA coupling. The complete set of decoupled frequencies is shown in Fig. 5. The dispersion of the free-mode damping and coupling parameters is given in Fig. 6.

DISCUSSION

The ω_{TO1}, γ_{TO1}, $\gamma_{TO1\text{-}TO2}$, and ω_{TO2} parameters, when extrapolated to the zone center, are in excellent agreement with those determined from a similar analysis of the Raman scattering results (shown as open diamonds in Figs 5 and 6). This agreement for ω_{TO1} resolves the long-standing discrepancy between the Raman and neutron determinations of the ferroelectric mode frequency in orthorhombic $KNbO_3$.

It also shows that a coherent interpretation of the observed spectra can be obtained using purely dissipative mode-mode interactions: In the wave-vector range $0.1<\zeta<0.25$, we have shown that the dominant interaction mechanism between TO1 and TO2, and between TO1 and TA, is dissipative. We have assumed that this continue to be the case for $\zeta<0.1$, between TO1 and TA.

We note in Fig. 6 that both γ_{TA} and $\gamma_{TA\text{-}TO1}$ vanish in the low-q limit. This is expected, although not for symmetry reasons, but because of the nature of the atomic displacements involved in long-wavelength acoustic modes (viscous damping).

Finally we should point out that the parameter values plotted in Figs. 5 and 6 have not been corrected for the effects of finite instrumental resolution. These corrections are negligible for the mode frequencies shown in Fig. 5 and for the soft-mode damping γ_{TO1}, the latter being much larger than the instrumental linewidth. On the other hand, the values given for γ_{TA} and γ_{TO2} are overestimated by about 0.2 and 0.4 THz, respectively. As a result, the consistency between Raman and neutron scattering estimates for γ_{TO2} is probably better than shown in the figure. Another effect of instrumental resolution is to wash out the asymmetrical (antiresonance) line-shape distortions which characterize mode interactions, leading to

an underestimation of the mode-coupling strengths. This effect is probably significant for $\gamma_{\text{TA-TO1}}$ at low q and for $\gamma_{\text{TO1-TO2}}$ at large q.

We see in Fig. 4(c) that the interference between TA and TO1 is destructive in the overlap region ($\omega_{\text{AT}} < \omega < \omega_{\text{TO1}}$), in the sense that the observed response is lower than calculated using independent oscillators. ITs effect is thus to lower the apparent frequency of the TA mode, as shown by the position of the lower dotted line in Fig. 5. In principle, the converse effect is expected for the TO1 frequency, contrary to what is observed (upper dotted line) in the figure. The reason for this lies in the strong damping of the TO1 mode at low q's, which produces a large shift in the apparent peak position to lower frequencies, thus canceling the small upward shift to the mode interaction.

ACKNOWLEDGMENTS

We wish to thank E. Weisendanger for the excellent single-crystal sample. The work of Northeastern University was supported initially by National Science Foundation (NSF) Grant No. DMR75-06789 and in the final stages by NSF Grant No. DMR-8604706. We also acknowledge partial travel support under NATO Grant No. 1360. Financial support was also provided for H.B. by the Max Planck Institute Hochfeldmagnetlabor, Grenoble and for C.H.P. by the Humboldt Foundation.

---

*Present address: Westinghouse Research and Development, Pittsburgh, PA 15235.

†Present address: Rectorat de Versailles, 78000–Versailles, France.

[1]R. Comès, M. Lambert, and A. Guinier, Acta Crystallogr. A **26**, 244 (1970).

[2]R. Currat, R. Gomès, B. Dorner, and E. Weisendanger, J. Phys. C 7, 2521 (1974).

[3]C. H. Perry, R. R. Hayes, and N. E, Tornberg, *Proceedings of the Second International Conference on Light Scattering in Solids, Campinas, Brazil, 1975,* edited by M. Balkanski *et al.* (Flammarion, Paris, 1975), p. 812.

[4]T. Fukumoto, A. Okamoto, T. Hattori, A. Mitsuishi, and T. Fukuda, Solid State Commun. **17**, 427 (1975).

[5]D. G. Bozinis and J. P. Hurrell, Phys. Rev. B **13**, 3109 (1976).

[6]A. M. Quittet, M. I. Bell, M. Krauzman, and P. M. Raccah, Phys. Rev. B **14**, 5068 (1976).

[7]A. M. Quittet, J. L. Servoin, and F. Gervais, J. Phys. **42**, 493 (1981).

[8]M. D. Fontana, A. Ridah, G. E. Kugel, and C. Carabatos-Nedelc, J. Phys. C **21**, 5853 (1988).

[9]M. D. Fontana, G. Métrat, J. L. Servoin, and F. Gervais, J. Phys. C **16**, 483 (1984).

[10]C. H. Perry, H. Buhay, A. M. Quittet, and R. Currat, *Proceedings of the International Conference on Lattice Dynamics, Paris, 1977,* edited by M. Balkansi (Flammarion, Paris, 1978), p. 677; H. Buhay, C. H. Perry, R. Currat, and A. M. Quittet, Bull. Am. Phys. Soc. **30**, 527 (1985).

[11]J. F. Scott, Phys. Rev. B **15**, 2826 (1977).

[12]J. P. Hurrell and D. G. Bozinis, Solid State Commun. **17**, 1541 (1975).

[13]F. Gervais, Opt. Commun. **22**, 116 (1977).

[14]R. M. Migoni, H. Bilz, and D. Bauerle, Phys. Rev. Lett. **37**, 1155 (1976).

[15]M. D. Fontana, G. E. Kugel, and C. Carabatos, J. Phys. **42**, C6, 749 (1981).

[16]C. H. Perry, R. Currat, H. Buhay, R. M. Migoni, W. G. Stirling, and J. D. Axe, Phys. Rev. B **39**, 8666 (1989).

[17]J. Harada, J. D. Axe, and G. Shirane, Phys. Rev. B **4**, 155 (1971).

[18]H. Vogt, J. A. Sanjurjo, and G. Rossbroich, Phys. Rev. B **26**, 5904 (1982).

[19]A. C. Nunes, J. D. Axe, and G. Shirane, Ferroelectrics **2**, 291 (1971).

[20]H. Vogt, M. D. Fontana, G. E. Kugel, and P. Gunter, Phys. Rev. B **34**, 410 (1986).

[21]K. A. Müller and W. Berlinger, Phys. Rev. B **34**, 6130 (1986).

[22]R. A. Cowley, Adv. Phys. **12**, 421 (1963).

[23]A. S. Barker and J. J. Hopfield, Phys. Rev. **135**, A1732 (1964).

[24]R. K. Wehner and E. F. Steigmeier, RCA Rev. **36**, 70 (1975).